

**Climatology, seasonality and trends of oceanic coherent
eddies**

Josué Martínez-Moreno¹, Andrew McC. Hogg¹, and Matthew England²

⁴ Research School of Earth Science and ARC Center of Excellence for Climate Extremes, Australian
⁵ National University, Canberra, Australia

⁶ Climate Change Research Centre (CCRC), UNSW Australia, Sydney NSW, Australia

Key Points:

- ⁸ Kinetic energy of coherent eddies contain around 30% of the surface ocean kinetic
⁹ energy budget.
- ¹⁰ Seasonal cycle of the number of coherent eddies and coherent eddy amplitude re-
¹¹ veal a 3-6 month lag to wind forcing
- ¹² The coherent eddy amplitude has increase at a rate of 3 cm per decade since 1993.

13 **Abstract**

14 Ocean eddies influence regional and global climate through mixing and transport
 15 of heat and properties. One of the most recognizable and ubiquitous feature of oceanic
 16 eddies are vortices with spatial scales of tens to hundreds of kilometers, frequently re-
 17 ferred as “mesoscale eddies” or “coherent eddies”. Coherent eddies are known to trans-
 18 port properties across the ocean and to locally affect near-surface wind, cloud proper-
 19 ties and rainfall patterns. Although coherent eddies are ubiquitous, yet their climatol-
 20 ogy, seasonality and long-term temporal evolution remains poorly understood. Thus, we
 21 examine the kinetic energy contained by coherent eddies and we present the annual, in-
 22 terannual, and long-term changes of automatically identified coherent eddies from satel-
 23 lite observations and a state of the art numerical simulation from 1993 to 2018. Satel-
 24 lite observations show that around 40% of the kinetic energy contained by ocean eddies
 25 corresponds to coherent eddies. Additionally, a strong hemispherical seasonal cycle is ob-
 26 served, on top of a 3–6 months lag between the wind forcing and the response of the co-
 27 herent eddy field. Furthermore, the seasonality of the number of coherent eddies and their
 28 amplitude reveals that the number of coherent eddies responds faster to the forcing (~ 3
 29 months), while the coherent eddy amplitude is lagged by ~ 6 months. There are regions
 30 that show a pronounced influence of coherent eddies, notably, the East Indian Ocean,
 31 the East Tropical Pacific Ocean, and the South Atlantic Ocean. In these locations, a strong
 32 seasonal cycle and interannual variability can be observed in both satellite and numer-
 33 ical models. Although, there is agreement between these products on the seasonality of
 34 the number of eddies, the seasonality of the coherent eddy amplitude between these prod-
 35 ucts show some inconsistencies. Long-term trends of the coherent eddy amplitude from
 36 satellite observations and the state of the art model show significant increases in the eddy
 37 amplitude of $\sim 3\text{cm}$ per decade in large portions of the ocean, while the number of co-
 38 herent eddies remains constant. Our analysis highlight the relative importance of the co-
 39 herent eddy fiend in the ocean kinetic energy budget, imply a strong response of the eddy
 40 number and eddy amplitude to the surface wind at different time-scales, and showcases
 41 for the first time seasonality, and multidecadal trends of the coherent eddy properties.

42 **Plain languange summary**

43 **1 Introduction**

44 Mesoscale ocean variability with spatial scales of tens to hundreds of kilometers is
 45 the most energetic scale in the ocean and comprises processes such as vortices, waves,
 46 and jets. In particular, one of the most recognizable mesoscale process are vortices. Al-
 47 though, in literature mesoscale vortices are commonly refer as "mesoscale eddies", this
 48 term is often used to describe mesoscale ocean variability, thus, where we will use the
 49 term coherent eddy to refer to coherent vortices.

50 Coherent eddies bla bla bla

51 **2 Methods**

52 **2.1 Kinetic Energy decomposition**

53 Kinetic energy is commonly divided into the mean and temporal variability com-
 54 ponents through a Reynolds decomposition. At a given time, the velocity field (\mathbf{u}) is split
 55 into the time mean ($\bar{\mathbf{u}}$) and time varying components (\mathbf{u}'). Additionally, as part of the
 56 climatology we also further decompose the eddy kinetic energy into the eddy kinetic en-
 57 ergy contained by coherent features (\mathbf{u}'_e) and non-coherent (\mathbf{u}'_n). Therefore the KE equa-
 58 tion can be written as:

$$\text{KE} = \bar{\mathbf{u}}^2 + \underbrace{\mathbf{u}'_e^2 + \mathbf{u}'_n^2}_{\mathbf{u}'^2} + \mathcal{O}^2 \quad (1)$$

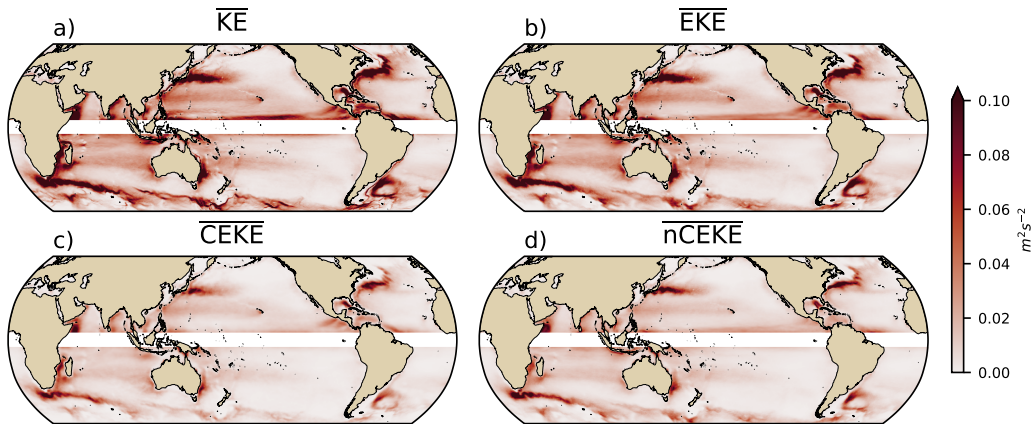
59 The second order terms (\mathcal{O}) are negligible as their time average is two orders of mag-
 60 nitude smaller than any other term. For more information about the decomposition of
 61 the field into coherent features and non-coherent features refer to Martínez-Moreno et
 62 al. (2019).

63 **3 Results**

64 **3.1 Coherent Eddy Energetics**

65 **3.1.1 Global**

- 69 • Figure 1 shows regions with high values of Kinetic Energy at the Western Bound-
 70 ary Currents, ACC, and ocean gyres.



66 **Figure 1.** Climatology of surface kinetic energy (\overline{KE}), surface eddy kinetic energy (\overline{EKE}),
 67 surface coherent eddy kinetic energy (\overline{CEKE}), and surface non-coherent eddy kinetic energy
 68 (\overline{nCEKE}) between 1993-2018.

- 71 • \overline{EKE} Explains 70% of \overline{KE} , while \overline{CEKE} is 40% of \overline{EKE} and \overline{nCEKE} is 60% of
 72 \overline{EKE}
 73 • Maps show that \overline{KE} , \overline{EKE} , \overline{CEKE} , and \overline{nCEKE} are dominated by the western bound-
 74 ary currents, the Antarctic Circumpolar Current (ACC).

82 Note that $nCEKE$ has a large amount of energy at high latitudes, this could be a
 83 consequence of the satellites not resolving the mesoscale coherent eddies.

84 *3.1.2 Seasonality*

92 **3.2 Coherent Eddy Statistics**

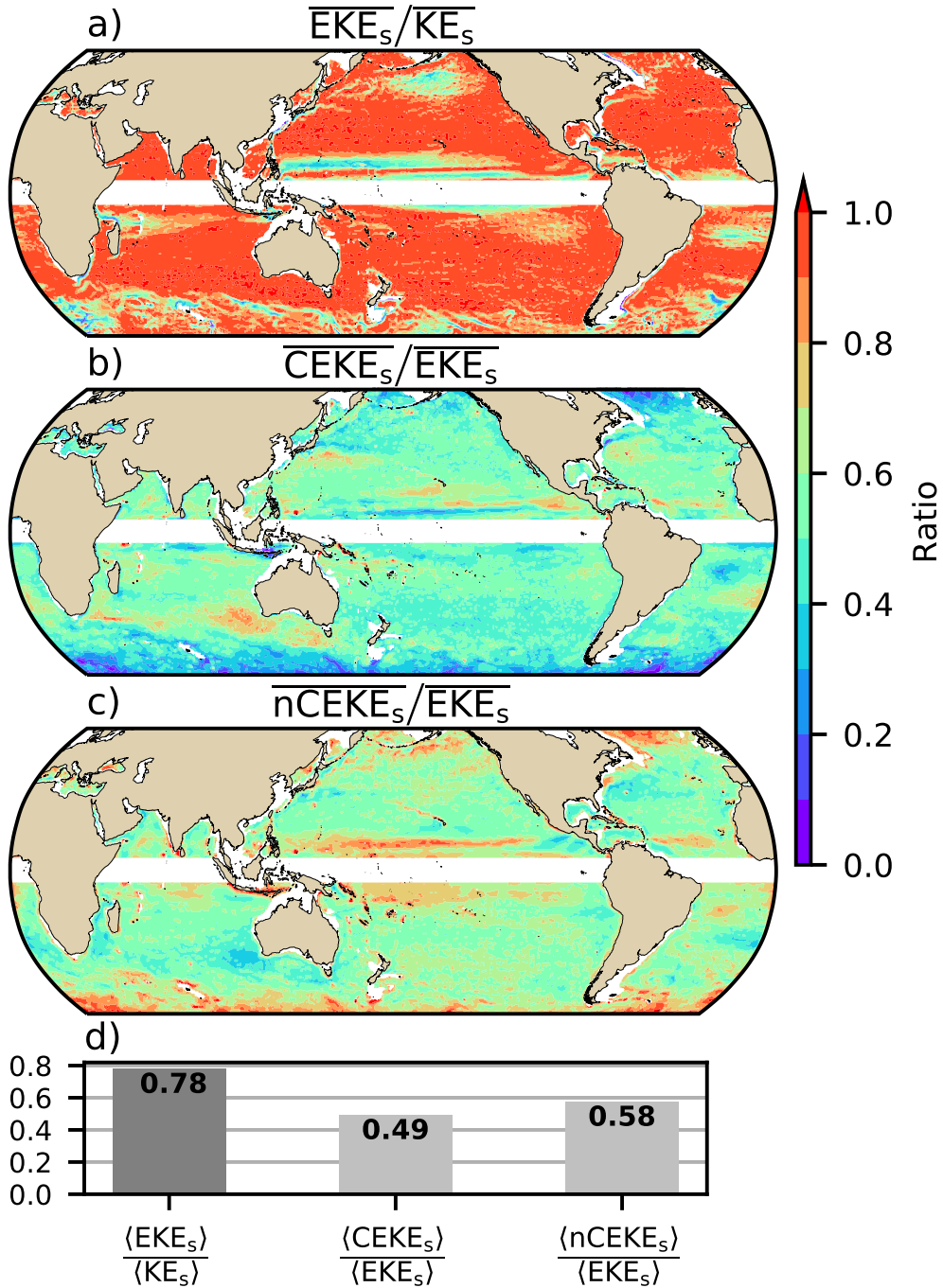
93 *3.2.1 Global*

94 **Make sure to mention dipoles in the boundary currents.**

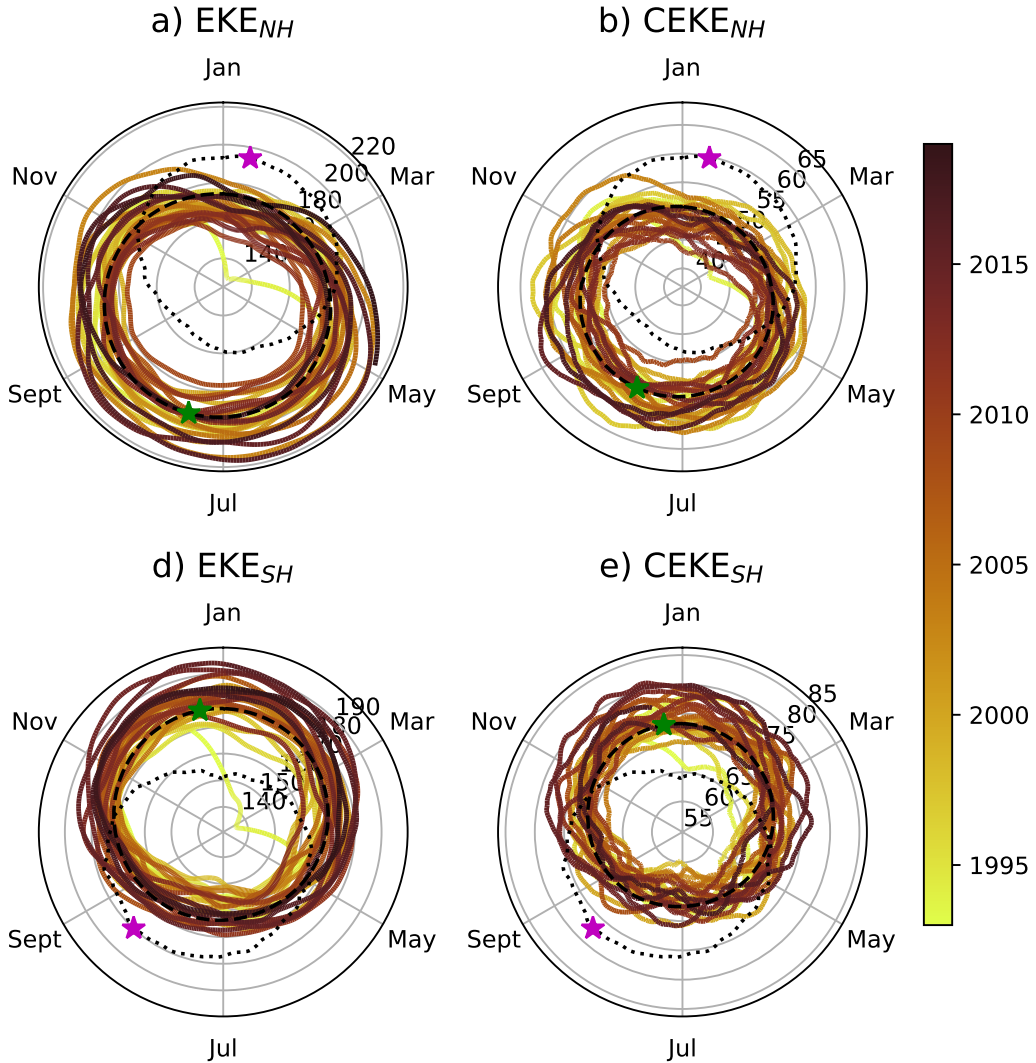
95 •

101 Although these algorithms use different identification criteria, the spatial pattern
 102 of the number of eddies is consistent between them.

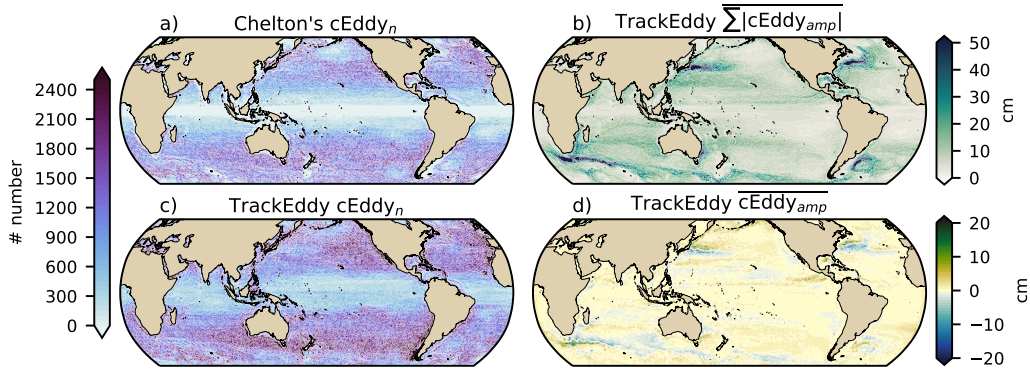
103 The maximum positive coherent eddy amplitude is commonly located polewards
 104 of the major boundary currents, while the maximum negative coherent eddy amplitude



75 **Figure 2.** Ratios of the kinetic energy components. a) Map of the proportion of mean eddy
 76 kinetic energy (EKE) versus mean kinetic energy (\overline{KE}); b) Map of the proportion of mean co-
 77 herent eddy kinetic energy (\overline{CEKE}) versus mean eddy kinetic energy (\overline{EKE}); c) Map of the
 78 proportion of mean non-coherent eddy kinetic energy (\overline{nCEKE}) versus mean eddy kinetic energy
 79 (\overline{EKE}); d) Global ratios of mean eddy kinetic energy ($\langle \overline{EKE} \rangle$), mean coherent eddy kinetic en-
 80 ergy ($\langle \overline{CEKE} \rangle$) and mean non coherent eddy kinetic energy ($\langle \overline{nCEKE} \rangle$) versus the global mean
 81 kinetic energy ($\langle \overline{KE} \rangle$) and global mean eddy kinetic energy ($\langle \overline{EKE} \rangle$).



85 **Figure 3.** Hemispherical seasonality of eddy kinetic energy (EKE), coherent eddy kinetic
 86 energy (CEKE), and non-coherent eddy kinetic energy (CEKE). Panels a,b and c show the
 87 northern hemisphere seasonal cycle, while panels d,e, and f correspond to the southern hemi-
 88 sphere. Dashed lines correspond to the seasonal climatology of the fields and dotted lines show
 89 the climatology of the wind magnitude. The green and magenta stars show the maximum of the
 90 seasonal cycle for the kinetic energy components and the wind magnitude, respectively. The line
 91 colors show the year.



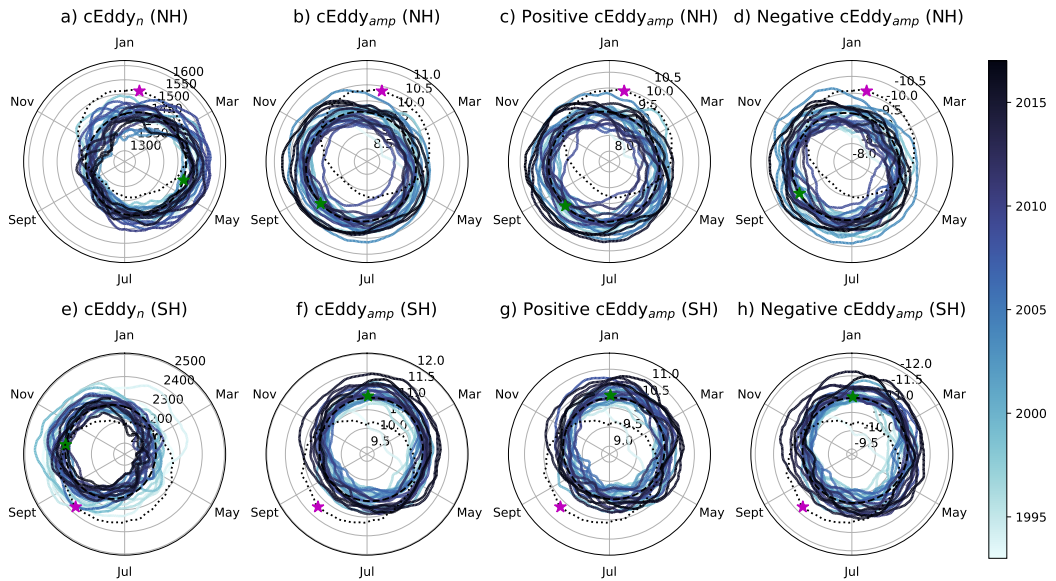
96 **Figure 4.** Climatology of the coherent eddy statistics. a) Climatology of the number of coherent
 97 eddies ($cEddy_n$) identified by Chelton et al. (2007); b) Climatology of the warm core coherent
 98 eddy amplitude ($cEddy_{amp}$). c) Climatology of the number of coherent eddies ($cEddy_n$) identified
 99 by Martínez-Moreno et al. (2019); d) Climatology of the cold core coherent eddy amplitude
 100 ($cEddy_{amp}$).

105 is found equatorwards. This is consistent to how coherent eddies are shed from these boundary currents.
 106

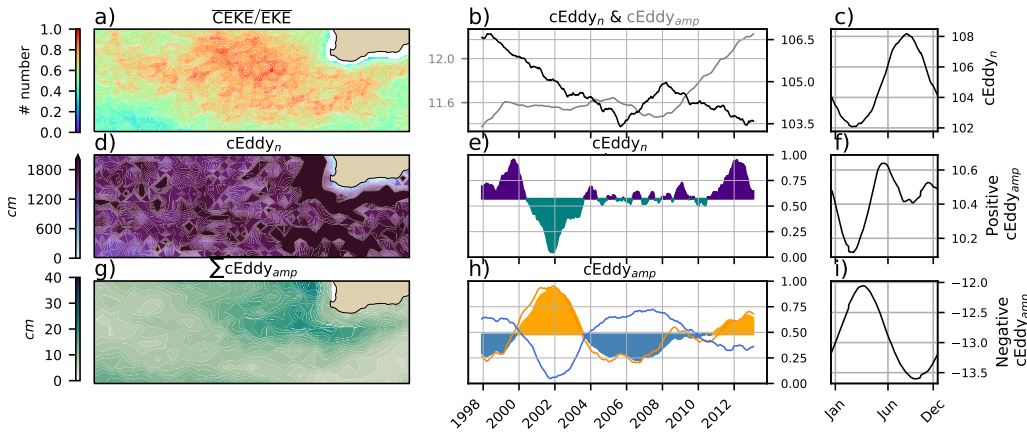
107 3.2.2 Seasonality

117 3.3 Regional

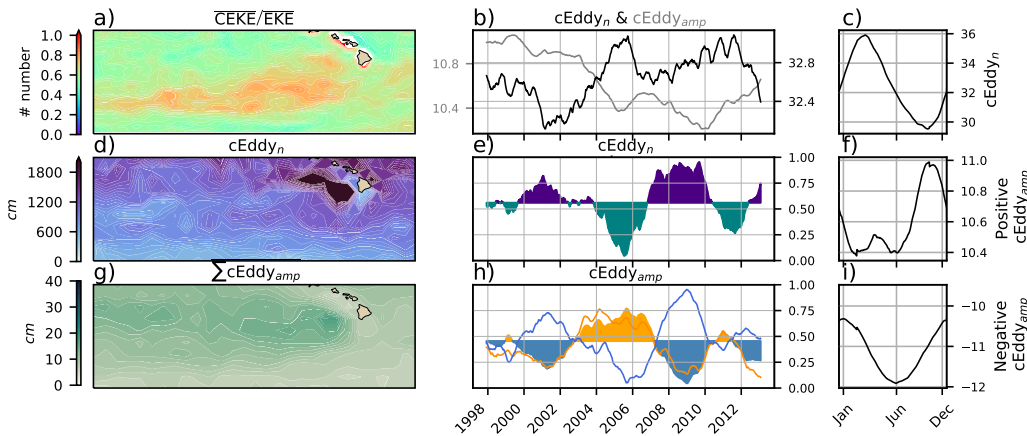
123 Number 295.85546403962104 Pos amp 0.12094501820533601 Neg amp -0.1385068018754378
 124 Chelton Number 236.7010877964295 Chelton Pos amp 7.779538694987785 Chelton Neg
 125 amp -10.075637745571715 ACCESS Number 315.24697840283096 ACCESS Pos amp 0.0875635001289238
 126 ACCESS Neg amp -0.08147261526708122
 127 Number 207.37973697877084 Pos amp 0.08901200544912018 Neg amp -0.08816744392087235
 128 Chelton Number 155.8983449906741 Chelton Pos amp 5.461227370020861 Chelton Neg
 129 amp -5.348246201100335 ACCESS Number 243.4991508883295 ACCESS Pos amp 0.05249108358772637
 130 ACCESS Neg amp -0.04136883487182314
 131 Number 228.35682569539446 Pos amp 0.084251050110757 Neg amp -0.08530413757977995
 132 Chelton Number 170.22168598454567 Chelton Pos amp 5.291564971943509 Chelton Neg
 133 amp -5.128095846325381 ACCESS Number 311.68099516009386 ACCESS Pos amp 0.06803317095123791
 134 ACCESS Neg amp -0.04969146684717923



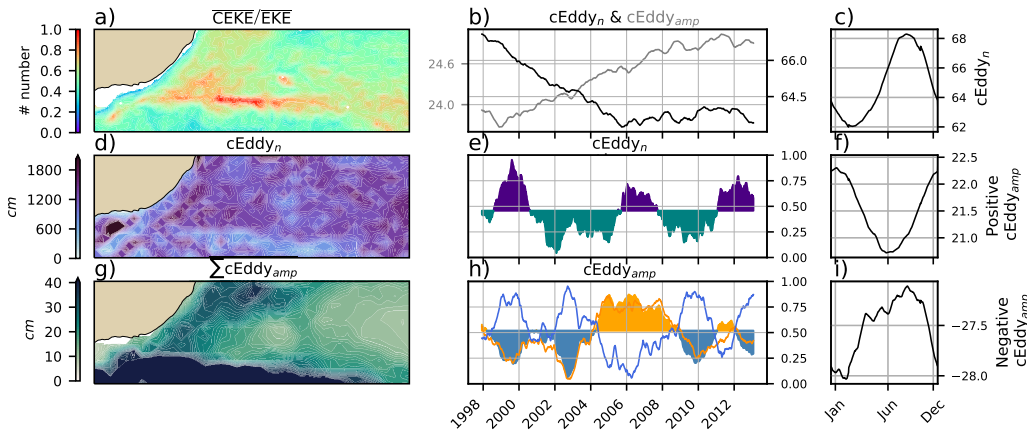
108 **Figure 5.** Hemispherical seasonality of the coherent eddy statistics; a,e) seasonal cycle of the
 109 number of coherent eddies ($cEddy_n$); b,f) seasonal cycle of the mean coherent eddy amplitude
 110 ($cEddy_{amp}$); c,g) seasonal cycle of the warm core coherent eddies amplitude ($wcEddy_{amp}$); d,h)
 111 seasonal cycle of the cold core coherent eddies amplitude ($ccEddy_{amp}$). Panels a,b and c show
 112 the northern hemisphere seasonal cycle, while panels d,e, and f correspond to the southern hemi-
 113 sphere. Dashed lines correspond to the seasonal climatology of the fields and dotted lines show
 114 the climatology of the wind magnitude. The green and magenta stars show the maximum of the
 115 seasonal cycle for the kinetic energy components and the wind magnitude, respectively. The line
 116 colors show the year.



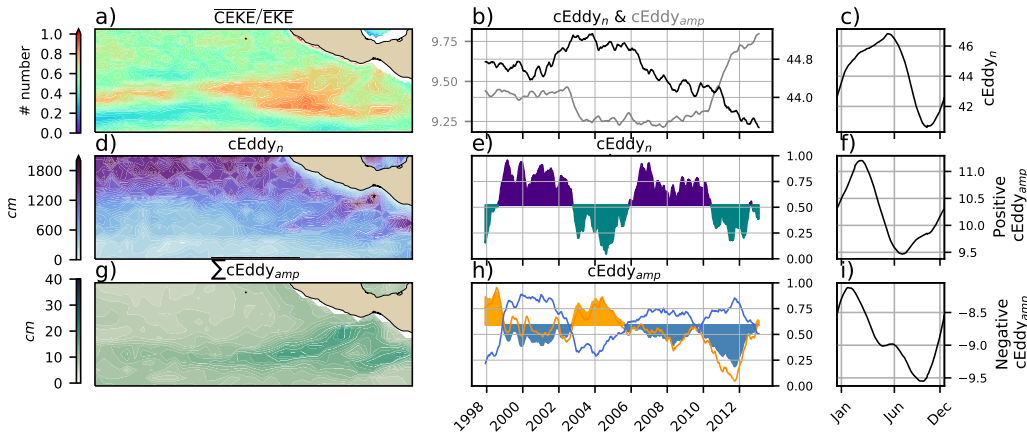
118 **Figure 6.** Climatology of regional statistics of the eddy field and coherent eddy field for the
 119 East Indian Ocean, East Tropical Pacific Ocean and South Atlantic Ocean. a-c Zoom to ratio of
 120 CEKE and EKE; d-f mean eddy kinetic energy ($\overline{\text{EKE}}$); g-i mean coherent eddy kinetic energy
 121 ($\overline{\text{CEKE}}$); j-k count of identified coherent eddies between 1993-2019; and l-n mean coherent eddy
 122 amplitude between 1993-2019.



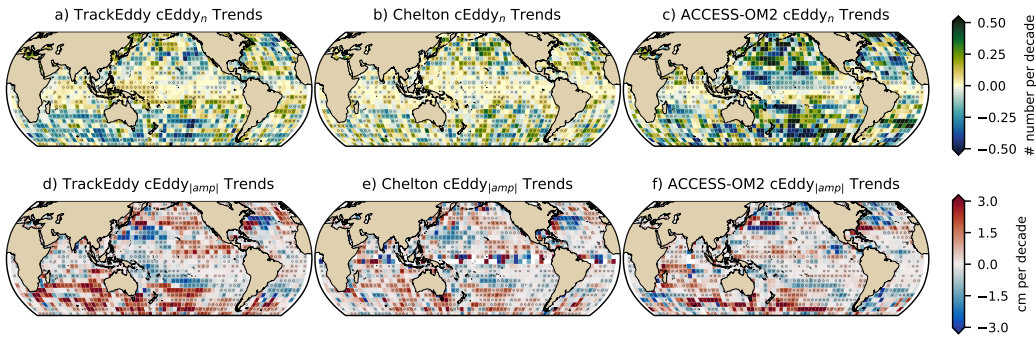
127 **Figure 7.** Climatology of regional statistics of the eddy field and coherent eddy field for the
 128 East Indian Ocean, East Tropical Pacific Ocean and South Atlantic Ocean. a-c Zoom to ratio of
 129 CEKE and EKE; d-f mean eddy kinetic energy ($\overline{\text{EKE}}$); g-i mean coherent eddy kinetic energy
 130 ($\overline{\text{CEKE}}$); j-k count of identified coherent eddies between 1993-2019; and l-n mean coherent eddy
 131 amplitude between 1993-2019.



136 **Figure 8.** Climatology of regional statistics of the eddy field and coherent eddy field for the
 137 East Indian Ocean, East Tropical Pacific Ocean and South Atlantic Ocean. a-c Zoom to ratio of
 138 CEKE and EKE; d-f mean eddy kinetic energy (\overline{EKE}); g-i mean coherent eddy kinetic energy
 139 (\overline{CEKE}); j-k count of identified coherent eddies between 1993-2019; and l-n mean coherent eddy
 140 amplitude between 1993-2019.



141 **Figure 9.** Climatology of regional statistics of the eddy field and coherent eddy field for the
 142 East Indian Ocean, East Tropical Pacific Ocean and South Atlantic Ocean. a-c Zoom to ratio of
 143 CEKE and EKE; d-f mean eddy kinetic energy (\overline{EKE}); g-i mean coherent eddy kinetic energy
 144 (\overline{CEKE}); j-k count of identified coherent eddies between 1993-2019; and l-n mean coherent eddy
 145 amplitude between 1993-2019.



153 **Figure 10.** Trends of coherent eddy statistics. a,b and c Trends of the number of identified
 154 coherent eddies from satellite observations identified using TrackEddy, satellite observations iden-
 155 tified using Chelton's, and state of the art numerical simulation identified using TrackEddy. d,e
 156 and f Trends of the sum of the absolute value of identified coherent eddies amplitude from satel-
 157 lite observations identified using TrackEddy, satellite observations identified using Chelton's, and
 158 state of the art numerical simulation identified using TrackEddy. Gray stippling shows regions
 159 that are statistically significant above the 95% confidence level.

150 Overall, we observe a polewards decrease in the number of the eddies. This sup-
 151 ports the idea that the satellite observations are consistent with a continue dataset.

152 **4 Trends**

160 **5 Summary and Conclusions**

161 **Acknowledgments**

162 **References**

- 163 Chelton, D. B., Schlax, M. G., Samelson, R. M., & de Szoeke, R. A. (2007). Global
 164 observations of large oceanic eddies. *Geophysical Research Letters*, 34(15),
 165 L15606. doi: 10.1029/2007GL030812
- 166 Martínez-Moreno, J., Hogg, A. M., Kiss, A. E., Constantinou, N. C., & Mor-
 167 rison, A. K. (2019). Kinetic energy of eddy-like features from sea surface
 168 altimetry. *Journal of Advances in Modeling Earth Systems*, 0(ja). doi:
 169 10.1029/2019MS001769